Received: 17 November 2020 | Revised: 15 January 2021 | Accepted: 15 January 2021

DOI: 10.1002/pen.25649

RESEARCH ARTICLE

spe INSPIRING PLASTICS PROFESSIONALS POLYMER ENGINEERING AND SCIENCE WILEY

Detection and evaluation of the fibers' deposition parameters during wet filament winding

Christian Hopmann | Nadine Magura | Nicolas Rozo Lopez | Daniel Schneider | Kai Fischer

Institute for Plastics Processing (IKV), RWTH Aachen University, Aachen, Germany

Correspondence
Nicolas Rozo Lopez, Institute for Plastics Processing (IKV), RWTH Aachen University, Seffenter Weg 201, Aachen 52074, Germany.
Email: nicolas.rozolopez@ikv.rwth-aachen.de

Funding information
German Bundesministerium für Verkehr und Digitale Infrastruktur, Grant/Award Number: 03B10104D

Abstract

Wet filament winding technology has been extensively used for the manufacture of rotationally symmetric parts made of fiber-reinforced plastics (FRP). As the design and modeling of FRP-parts require numerous assumptions, deviations between calculated and achieved mechanical properties are expected. One aspect that contributes to this discrepancy is the assumption of a homogeneous rectangular cross-section of the fiber-band. In this work, the fiber-band geometry in a wet-winding process of carbon fiber cylinders is analyzed. An Infrared-optical system for the detection of the fiber bandwidth and winding-angle is implemented. The influence of the winding speed and the resin temperature is analyzed. An image processing algorithm for the automatic measurement of the fiber's bandwidth and winding-angle is developed. Manual and adaptive gamma corrections are implemented to improve image quality. A parameter study for the suitable selection of image processing parameters is performed.

KEYWORDS

composites, imaging, orientation, processing, sensors

1 | INTRODUCTION

The conformation of tubes, driveshafts, vessels, and other rotational symmetric parts has been historically performed using filament winding technology.[1–4] In the last decades, with the demand for light-weight structures, carbon and glass fibers have been successfully integrated into different winding methods. For instance, in wet filament winding, where the fibers are impregnated with a low viscous resin as they are wound onto a rotating mandrel.[5] Furthermore, the winding pattern is usually a sequence of circumferential or/and helical layers. Thus, the laminate's mechanical properties depend not only on the influence of the process parameters but also on the number of layers, as well as their winding-angle.[6,7] For the design of complex winding structures, analytical models are restricted, and therefore, numerical approaches can be exploited.[8,9] Even though this manufacturing technology is well-known, the design and modeling of wound components require numerous assumptions and the repeatability of manufacturing is limited. Therefore, significant deviations in the mechanical properties of the manufactured parts in comparison to simulative predictions are expected. Consequently, high safety factors and/or over-dimensioning are usually applied to the components. For instance, for pressure vessels, the design is

Abbreviations: AFP, automated-fiber-placement; CFRP, carbon fiber-reinforced plastics; fps, frames per second; FRP, fiber reinforced plastics; FVF, fiber volume fraction; IR, infrared usually over-dimensioned above the high legal safety factor of 2.25.[10,11] This over-dimensioning leads to extra production costs since additional material is needed. Therefore, the goal must be to equalize the modeling and manufacturing of wound parts to become more material and cost-efficient.

An important aspect of this discrepancy between modeling and manufacturing is the assumption of the cross-section geometry of the fiber-band. Thus, for most of the simulation approaches, the cross-section is assumed to be rectangular and constant during the winding patterns. This assumption contradicts the process' reality where the fiber-band cross-section is variable, and its shape can be approached narrow elliptical rather than rectangular, especially with increasing width to thickness ratio. Moreover, during the fiber's deposition, which is accompanied by spreading, changes in the width of the fiber-band (bandwidth) occur. These bandwidth variations, as well as changes in the winding-angle, describe the formation of gaps or overlaps in the laminate structure. In addition, variations of the local fiber volume fraction (FVF) can be expected from the fluctuations in the fiber-band thickness, fiber-band slippage, or spreading. Since the variations of the bandwidth and winding-angle are important for improved modeling of the part performance, optical systems have been considered for the inline detection of these values within this work. Nowadays, image acquisition systems such as industrial cameras, or infrared-cameras (IR-camera) have a broad application in manufacturing processes.[12–14] For the manufacture of fiber-reinforced plastic (FRP)-tapes in automated fiber placement processes, IR-camera systems have shown good results for the fiber-band recognition due to the thermal difference of the incoming fiber-band and the deposition surface (background).[15–17] However, the quality of the image is highly dependent on the contrast between the tracking object, that is, fiber-band, and the background.[18–20]

This article intends to expand the understanding of the wet-winding of carbon fiber-reinforced plastics (CFRP) through the studying of the fiber-bandwidth and its winding-angle during a circumferential winding pattern. An IR-optical system is implemented and the influence of the winding speed and resin temperature on the acquired images are analyzed. An image processing algorithm for the automatic measurement and evaluation of the bandwidth and winding-angle is developed. This approach should serve as a basis for more accurate simulation of wound parts as well as support for the development of quality control methods.

2 | STATE OF THE ART

To further understand the wet filament winding process, the relevant state of the art is presented. Thus, the most important factors and assumptions are summarized. Furthermore, this overview defines the process basis for the evaluation of the fiber bandwidth and winding-angle.

2.1 | Wet filament winding manufacture process

Filament winding is a well-established manufacturing process for composites since 1940 and widely used for the manufacture of rotational-symmetric parts, in which pressure vessels for fuel cell-based drive have increased its demand.[1] A general wet filament winding process can be abstracted into three steps: Provision of fibers with a defined tension, fiber impregnation, and deposition around the winding body (Figure S1). In addition, a common practice after the process is the curing of the wound part.[2]

The process begins at the creel rack where individual rovings are pulled at a defined tension. At the impregnation unit, a liquid matrix material is transferred to the fibers by immersion, roller, pressure, or vacuum impregnation.[2,14,21] For the roller impregnation technique, the rovings are guided over a rotating roller, which is loaded with a defined resin film. Hence, the liquid matrix material flows through the rovings in the direction of thickness. The air contained can thus escape upwards and the impregnation quality increases. Furthermore, for a high impregnation quality, a low viscosity of the resin, for example, lower than 2 Pa s, as well as a spreading of the rovings are beneficial.[4] After the impregnation unit, the rovings are combined to form a fiber-band. The impregnated fiber-band is then placed on the winding body by a deposit roll or thread eye along the winding path.

The winding pattern is usually a sequence of helical and circumferential layers. Circumferential layers cover in a band-to-band deposition the cylindrical part of the pressure vessel and serve to absorb radial forces.[22] A high compression effect of this layer on the layers below is as characteristic as the possibility of high winding speeds up to 2.0 m/s. Helical layers, however, allow for more variations in the winding pattern due to different winding angles. These layers dominate the axial or the torsional strength of the part. Once, the part has been fully wound, the resin needs to cure. Depending on the resin used, this can take place under ambient conditions or in ovens. The component must rotate during this process to avoid dripping of the low-viscous resin and to ensure a homogeneous fiber-matrix distribution.[4]

2.2 | Fiber-band geometry in wet filament winding

The laminate is conformed by a sequence of circumferential and helical layers with different angles, which are determined usually by finite element simulations. Thus, by including the component's geometry and material properties, the mechanical performance of the part can be simulated. Furthermore, simulations of the winding path, which transfers the determined layup in machine code, can be used to support the manufacture of the part.

Regardless of the software used, the simulations can model the final component in detail, accurately in many cases. Nevertheless, within each layer, the fiber-band cross-section is usually assumed as rectangular with no changes in its geometry. However, for different winding patterns some parameters, such as FVF, can be adjusted to introduce differences in the mechanical properties. To account for a deviation of the fiber-band geometry from the rectangular cross-section, the fiber-band can be considered with a slight overlap instead of a band-to-band deposition. Based on these assumptions, the overlaps are estimated, and therefore, the real fiber-band geometry is not completely considered.

Despite the good modeling obtained with rectangular cross-sections of the fiber-band, some publications describe the bandwidth as an elliptical or half-elliptical cross-section in real terms.[23] By considering surface constancy for the fiber-band cross-section, the same heights of the fiber-band will lead to different fiber bandwidth and vice versa when considering a non-rectangular fiber-band. This assumption of an elliptical cross-section correlates well, with the deposition of slightly overlapping fiber-bands to achieve a homogenous FVF.

Moreover, the effect of fiber spreading will cause a change in fiber bandwidth when the fiber-band is deposited on the part. This also affects the cross-section of the fiber-band. However, the effect of fiber spreading will depend on the surface curvature of the winding body, the winding pattern, the fiber tension, and the wetting of the fibers with the viscous resin.[2,23,24] Therefore, the bandwidth on the winding body will show fluctuations, even, if considering rovings with no deviations, which does not apply to reality. These deviations from the modeled rectangular cross-section can lead to gaps and overlaps affecting the mechanical strength of a part.[25] As gaps and overlaps can result from fluctuations in bandwidth and winding-angle, a better understanding of the fiber-band geometry during wet winding is necessary. To identify fluctuations in these parameters during manufacturing a suitable inline measuring system is required. In wet filament winding, the bandwidth and winding-angle are defined by the two edges of the fiber-band (Figure 1). Therefore, the inline measurement needs to allow the detection of both edges during band-to-band deposition independent of the winding pattern of the background and the incoming fiber-band orientation.

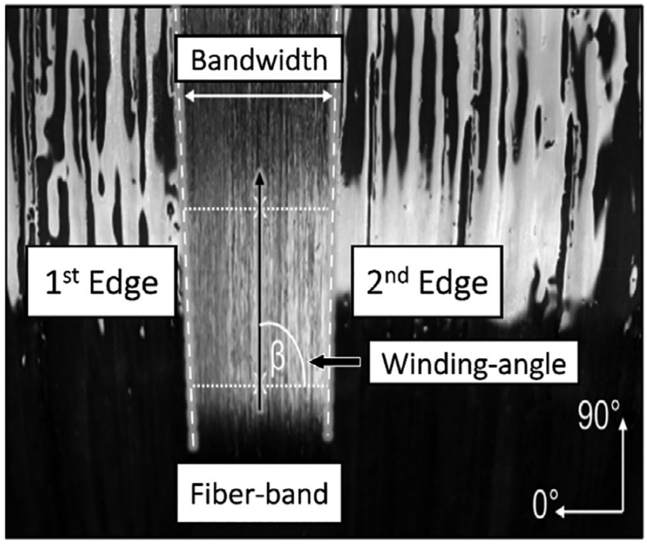

FIGURE 1 Definition of the fiber bandwidth, and the winding-angle by the two edges of the fiber-band

2.3 | Image acquisition approaches for fiber-band recognition

In related technologies as the automated-fiber-placement (AFP) process or the winding process with thermoplastic tape (tape-winding), optical inline measurement systems are already used. Even though the production speed, the usage of pre-impregnated tapes, and the part geometry differ significantly from wet filament winding, there are similarities as the local deposition of fiber-bands on a background of the same type and high reflectivity of the materials, which justify a profound look into these technologies.

Witte measured gaps between tapes during the tape winding process with the concept of interferometry.[26] This approach is based on well-defined edges of the thermoplastic tape after the deposition on the winding body. The vertical resolution of this scanning system is 0.84 μm and a vertical measuring range of 12 mm can be displayed.[27]

For the inline determination of critical defects concerning their type, size, and position, Colas et al. integrated an IR camera into the tape winding process.[28] In addition to superficial placement defects, intralaminar defects such as porosity and inhomogeneity in the tape should also be detected in the IR image. At measuring speeds of up to 7 m/min, gaps and overlaps during the tape deposition process could already be detected and visualized by further processing algorithms in a 3D reconstruction.

Due to its wide distribution in the aviation industry, there are numerous research initiatives and approaches for automated inline quality assurance in AFP processes. The determination of the placement position of the single thermoplastic or thermoset pre-impregnated tapes plays an important role. The resulting gaps and overlaps are detected by a laser-assisted recording of the height profile,[13,29–35] IR camera images,[12,14,16,21,36–39] as well as eddy current testing[37] or fiber Bragg sensors.[40,41] Laser and thermography methods are widely followed approaches.

Krombholz et al. have developed an inline system for detecting the edge position of each deposited fiber-band using a laser light section sensor.[42] Even though the system is designed for the AFP process, it was developed in a robot-assisted towpreg winding process. The detection of individual towpregs on an aluminum core could be performed with the sensors used.[42] However, the deposition of towpregs on a CFRP substrate resulted in difficulties as edge detection was made more difficult by the substrate, and the material deformation during deposition.[42] The sensor used was designed for the detection of towpregs with a height of approx. 125 μm at a deposition speed of up to 1 m/s. Using edge detection, the edge is mapped by a curved transition in deviation from the model conception of a right-angled jump. Within the scope of the investigations, two sensors were compared with each other and the influence of the laser intensity and the angle of incidence was worked out.

Brüning et al.[21] and Denkena et al.[15] worked with thermography for inline inspection. By implementing an IR-camera, the deposited tape is recorded behind the deposition point (first contact point of incoming fiber-band and winding body). The method is based on the approach that there is a significant temperature difference between the substrate and the freshly deposited tapes. The temperature difference between the deposited tape and the base substrate is used to determine the edges of the tape. The tape is even colder than the substrate when deposited just behind the pressure roller. An algorithm determines the tape geometry from the data by evaluating the thermal profile, from which manufacturing defects (gaps greater than 0.7 mm, overlaps, twisted tows) can be deduced with near real-time resolution. By correlation with the coordinates of the deposition robot, a local resolution and thus a target/actual comparison is also possible. Gaps and overlaps can be separated from each other from the temperature profile. While overlaps lead to a lower temperature, gaps show the temperature of the substrate in the line profile of the temperature. For a clear determination of the tower edges on both sides with this measuring principle, a small gap between adjacent bands is necessary. To detect surface defects such as contamination and changes in the surface material, the edge detection method is combined with a surface inspection based on the evaluation of temperature peculiarities.[12,13,21,36]

Gregory et al.[38] of the NASA Langley Research Center see an essential advantage of thermography compared to laser-based detection in the possibility to identify poor layer bonding/consolidation besides gaps, overlaps, and fiber twist, additional defects by detailed analysis of the temperature profile. By considering the local heat flow, the heat signal can be traced back to the individual defect patterns. An IR camera with 640 × 512-pixel resolution and a measuring rate of up to 30 Hz is used for this purpose, which records the material deposit directly behind the tape deposition. By integrating the camera into the depositing head, each recorded image can theoretically be assigned to a position on the component using the robot coordinates. Within the scope of this work, however, a correlation is carried out here by assuming constant travel speeds. By evaluation of the thermographic images, areas with reduced connection to both plates and cylindrical components could be successfully detected.

2.4 | Selection of image acquisition technology for wet filament winding

The literature review shows that several optical systems can be considered for the quality control of the manufacturing process as AFP or tape-winding.[36,39,40,43,44] These options can be classified into two groups: direct measure systems and image acquisition systems. One of the most popular direct measurement systems is the linear laser scanner. This method has shown accurate results for the recognition of some object surface and profile's edge detection as stated above. However, limitations occur if the height profile of the deposited fiber-band is not well defined. As both edges need to be captured for the determination of the bandwidth, a suitable band-to-band deposition is not possible. This requirement excludes some technologies as the interferometry performed by *Witte*.[26] Considering the cross-section of the fiber-band as an elliptical or half-elliptical area there will be hardly any recognizable edge in the heights profile of the winding body (Figure 2). In contrast to thermoplastic or thermoset tapes in AFP, the deposited material in the wet winding homogenizes with the background at the deposition point, so that no edge detection in a height profile will be possible.

On the other hand, due to the large amount of data collected, and its flexible integration into different processes, image acquisition systems have shown a broad application in the evaluation of composite materials.[38,43–45] Thermographic monitoring systems have shown promising results for the detection of process relevant defects in composite manufacturing.[12,14–17,46, 47] Nevertheless, a challenge for its implementation is

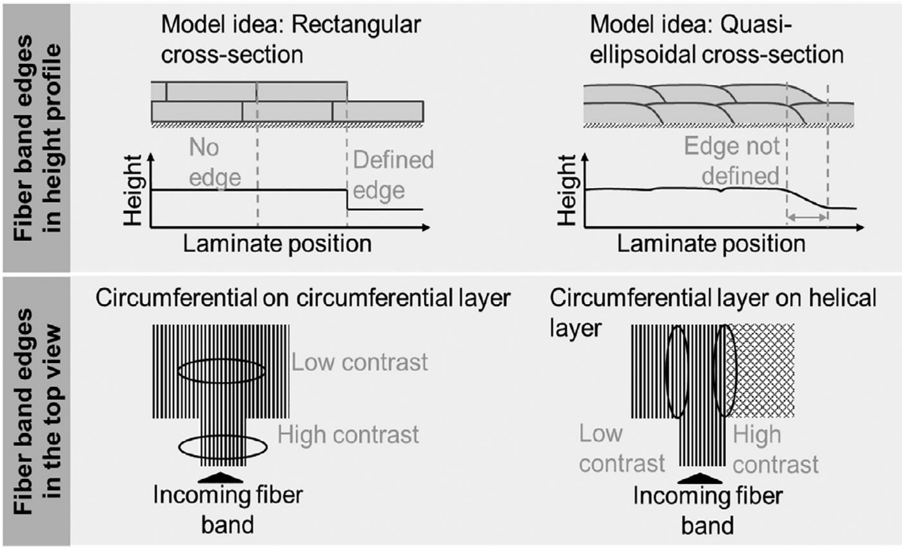

FIGURE 2 Characteristics of band-to-band deposition in wet filament winding depicting constraints for the selection of a suitable measurement approach for the determination of the fiber-band edges

the image quality.[46,47] To guaranty the image quality during a real process condition, a suitable image filter process is, therefore, required. To the authors' best knowledge, such IR-image filters have been not reported for a wet filament winding. Nevertheless, some algorithms for the improvement of IR-images have been already developed.[19,48–50] This kind of approach could be integrated to an IR-image system in a wet filament winding. However, further insight of the process conditions and its parameter is required to develop a suitable image process algorithm.

3 | EXPERIMENTAL EVALUATION OF TEMPERATURE CONTRAST DURING FIBER-BAND DEPOSITION

For the inline determination of the bandwidth and winding-angle, the suitability of the IF-camera is investigated. Furthermore, the fiber-band's edges can only be identified if an adequate temperature contrast is obtained.

For the investigations, a circumferential layer on a closed winding layer (here: substrate) with a band-to-band deposition is considered. It is assumed that the substrate has already time to cool down and then a temperature contrast to the incoming fiber-band is obtained. The bandwidth in the direction of deposition should, therefore, always show a well-defined (sharp) flank in the temperature profile. On the other hand, the opposite edge of the fiber-band, that is, opposite to the direction of deposition, is placed directly next to the fiber-band deposited shortly before, so that the cooling time is limited to one revolution of the winding body. In the following, we will, therefore, examine the effect of the winding speed and the temperature of the resin on the temperature contrast of both edges of the incoming fiber-band. Those two process parameters are chosen as both directly affect the temperature of the incoming fiber-band by the original temperature or in case of speed the dwell time, and therefore, the cooling before deposition. Moreover, the winding speed determined the time for one revolution of the winding body, and therefore, the cooling time of the previously placed fiber-band. In particular, the possibility is investigated that at high winding speeds and small diameters of the winding body, a loss of contrast can occur, which would characterize a limit of use of the measuring approach. Moreover, a minimal temperature may be needed to see a temperature contrast of the incoming fiber-band.

Therefore, in this chapter, the general suitability of the IR camera is tested for different winding speeds and rein bath temperatures. If the results are promising, an image processing algorithm for the determination of the fiber bandwidth and winding-angle is developed afterward.

3.1 | Experimental setup and image acquisition

For this work, the experiments are carried out on a portal winding machine type WSE IV, manufactured by Josef BAER Maschinenfabrik (Weingarten, Germany) with state-of-the-art materials. A thermoplastic cylinder of a 200 mm diameter is used as the winding mandrel. Carbon fiber rovings of the type ITS50 (1600 tex, 24 k) by Teijin Carbon Europe GmbH (Wuppertal, Germany) are impregnated and wrapped around the mandrel. Epoxy resin EPIKOTE Resin 04976 from Hexion Inc. (Columbus, Ohio) with a viscosity of 180 ± 30 mPas at 60°C is used. A free path length of 138 cm from the roller in the impregnation unit to the deposition point is measured. In all trials, a single roving is deposited. A bandwidth of approximately 10 mm at the deposition point is expected.

An A655sc IR-camera from FLIR Systems Inc. (Wilsonville, Oregon) with an image resolution of 640 × 480 pixels is used. The recording speed is set up to 50 frames per second (fps). The camera sensor measures in the IR-spectrum from 7.5 to 14 μm wavelength. In addition, the camera is equipped with a standard 25° lens with a resolution of 170 μm at a working distance of 250 mm. For the experimental setup, the camera is placed perpendicularly above the deposition point (Figure 3, left). For this setup, an example IR-image with the characteristics features during the winding process is presented (Figure 3, right). As the winding direction is from the left to the right, the previously wound area has a higher temperature in comparison to the last deposited layer. Thus, a longer cooling time for the right side is observed. For each test, the process is continuously recorded, and a video sequence with about 1000 frames is obtained. For the reported average values and standard deviations, the temperatures in all the frames are considered.

For evaluation of the IR image, either a gray value analysis or a temperature profile is possible. To examine the suitability of the measurement method, the temperature profile along the deposition line is then considered. Furthermore, the deposition point is estimated at pixel 400. For the image analysis, a python script for the characterization of the image values from the IR-camera has been written. Thus, the incoming fiber-band has a higher temperature in comparison to the background (Figure 4). Moreover, the temperature for the previously wound area (left hand to the winding direction) is higher in comparison to the temperature at the last layer region (right hand to the winding direction). For the estimation of ΔT in both sides of the fiber-band ($\Delta T_{incoming}$ and $\Delta T_{phase\text{-}out}$), the maximum temperature at the fiber-band (ΔT_{max}), and the mean temperature for 100 pixels after the fiber-band edge are considered. For the relative error of ΔT, the square root of the sum of squared standard deviations (standard deviation of ΔT_{max}, the standard deviation of the average value of the 100 pixels in the incoming or phase-out area, and its mean standard deviation) is considered.

Therefore, the fiber-band is determined by the step rise or fall of the temperature in the temperature profile, which does not perfectly correlate with the fiber bandwidth, but allows for the calculation of ΔT. The fluctuation range, indicated by the standard deviation of the mean value over 100 pixels in the incoming or phase-out area, describes the uniformity of the temperature profile. Thus, this value is giving an estimation of the risk to falsely detect other peaks as the fiber-band edges. Therefore, a low fluctuation width is a good indication for a well-defined fiber-band edge.

3.2 | Influence of the winding speed on the temperature contrast

The experiment shows that the previously wound area appears warmer at higher winding speeds (0.96 m/s) than at slow speeds (0.28 m/s) (Figure 5(A)). Therefore, the contrast in the incoming flank of the temperature profile

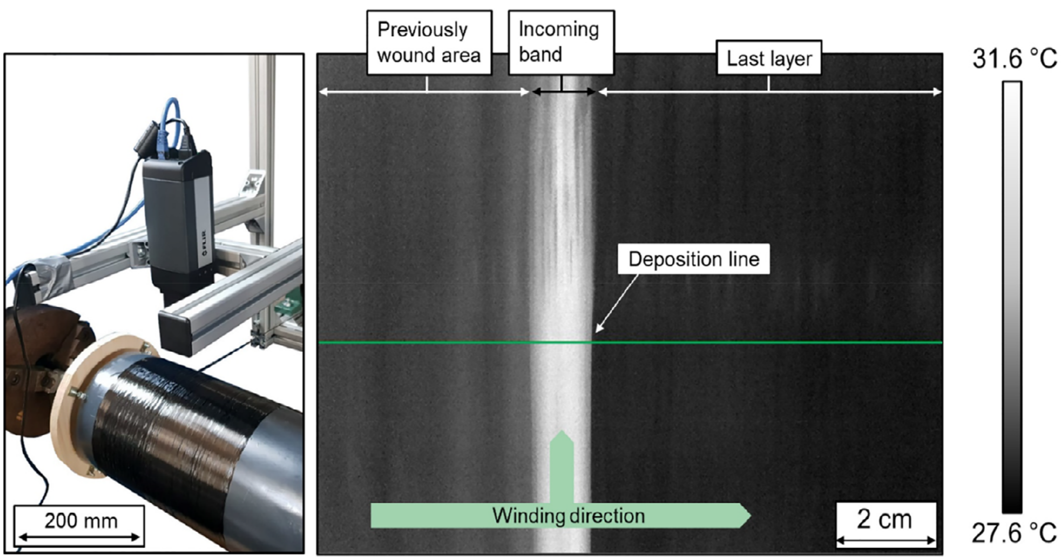

FIGURE 3 Experimental setup of the image acquisition system (left). Characteristic features of the recorded infrared images (right) [Color figure can be viewed at wileyonlinelibrary.com]

could become more difficult to analyze due to the lower contrast. Moreover, the absolute temperature of the incoming fiber-band is lower due to the longer dwell time between impregnation and deposition.

These results are depicted for different winding speeds (Figure 5(B)). The data show an increase of both ΔT values with increasing winding speed up to 0.7 m/s. Afterward, the values remain almost constant up to the maximum measured value of 0.96 m/s. In the future, it remains to be investigated how this curve will develop further for higher winding speeds above 1 m/s. On the "phased-out" flank, the fluctuation range is nearly constant, and therefore, the ratio of fluctuation range and ΔT shows a decreasing trend with the winding speeds as ΔT is increasing. As this ratio is for the quantification of the relative error value, no standard deviation is given.

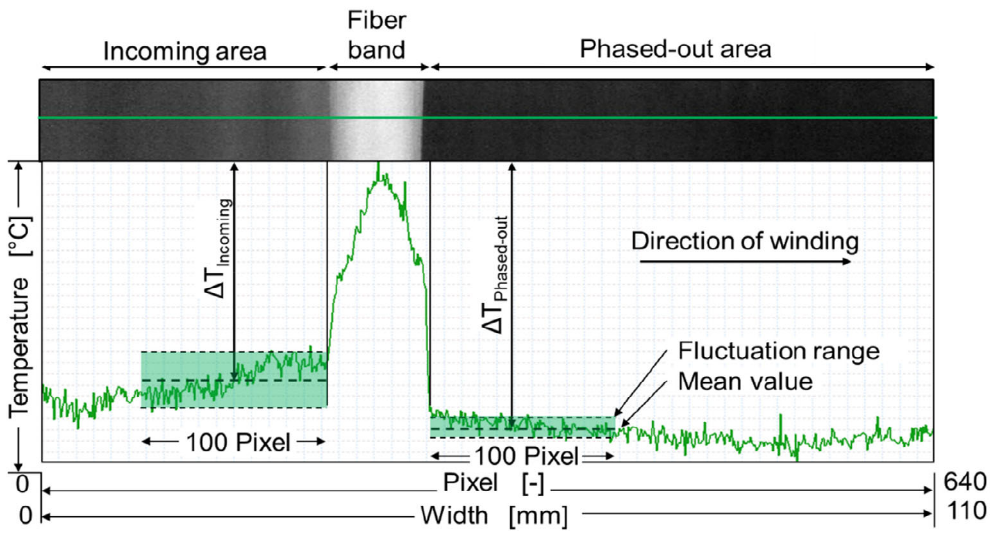

FIGURE 4 Determination of values for data evaluation from the line profiles of the infrared images [Color figure can be viewed at wileyonlinelibrary.com]

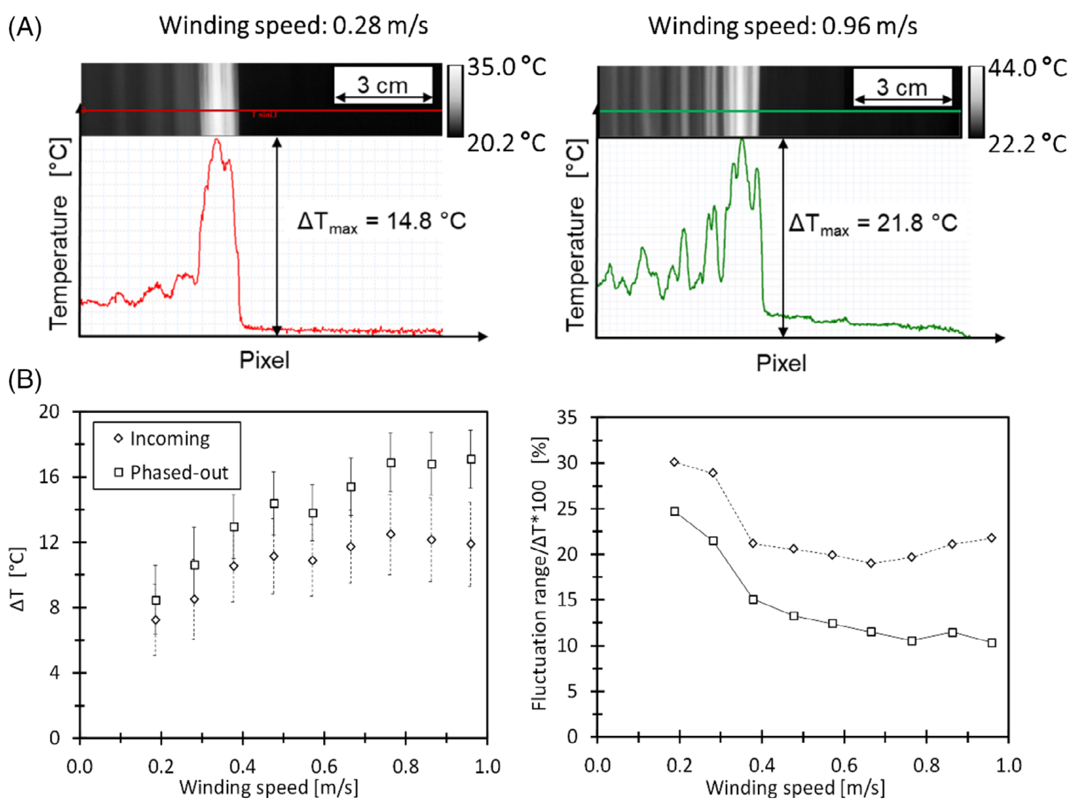

FIGURE 5 (A) Exemplary temperature profiles at winding speeds of 0.28 and 0.96 m/s.[52] (B) The influence of the winding speed on the measurement data of the circumferential winding. The values are estimated for the complete video recorded (temperature profile at pixel 400, with resin bath temperature: 60°C) [Color figure can be viewed at wileyonlinelibrary.com]

On the incoming flank, however, the curve shows a minimum in the range of 0.7 m/s. The high ratio at low winding speeds results from the low absolute value of ΔT. For high winding speeds above 0.7 m/s, however, the fluctuation range increases significantly resulting in a reduction of contrast on the incoming flank. For high speeds, even higher ratios are expected, which will make the automatic calculation of the bandwidth more challenging.

During the development of a suitable detection algorithm, the minimal requirement for the ratio between fluctuation range and ΔT must be determined, as this would limit the suitability of the measurement technology to certain winding speeds. Anyhow, the determined ΔT values above 8°C promise enough contrast on both edges for automated processing algorithms by visual inspection. Moreover, the determined trends need to be repeated for a winding pattern, in which fiber-band deposition is performed with a defined overlap, as higher ratios are expected.

3.3 | Impact of the resin bath temperature on the temperature contrast

The influence of the resin bath temperature on the temperature profile of the IR images is investigated (Figure 6). Increasing resin temperature results in a higher value of ΔT. Same as in the influence of the winding speed (Figure 5(B)), the incoming value of ΔT is always lower than the phased-out one, as assumed. For resin bath temperatures above 60°C, the fluctuation range has a more significant influence on the absolute flank height than for temperatures below 60°C. Thus, moderate resin bath temperatures between 40 and 60°C will be beneficial for the data evaluation for this specific setup.

The experimental results indicate the suitability of the IR camera for the wet filament winding process. However, limitations are expected for high winding speeds and winding patterns calculated with overlap as the temperature contrast on the phased-out flank will decrease. Thus, to further extend the evaluation and the suitability of an IR system, winding speeds above 1.0 m/s shall be additionally investigated. Common resin bath temperatures around 40–60°C are beneficial for the analysis, and therefore, are in good agreement with the approach. In the following, an image processing algorithm for the determination of the bandwidth is evaluated.

4 | DETERMINATION OF THE FIBER BANDWIDTH BY AN IMAGE PROCESSING ALGORITHM

The information obtained by the IR-camera is used for the automatic determination of the bandwidth and its winding-angle. For image processing standards, a gray-scale notation is used. Thus, the absolute black, and white in the image, that is,. minimum and maximum temperatures, are represented by the values 0 and 255, respectively. An image processing algorithm, supported by the OpenCV library, is developed in Python. In the image window, three regions are defined for the evaluation of the bandwidth and its winding-angle along the fiber-band. These are classified as upper-, middle-, and lower-region, (Figure 7). The upper-, and lower-region consist of two line-regions, located at 10 and 30 pixels from the external border. The middle-region is defined at the center of the image where the two line-regions are located at 10 pixels from the center. Thus, the distance between line-regions is 20 pixels for all the regions. To obtain the bandwidth, an edge-point is defined

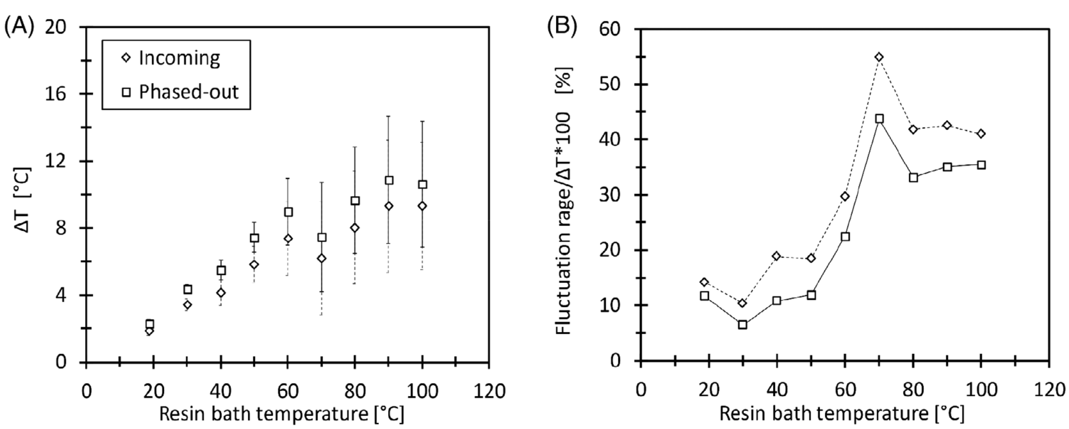

FIGURE 6 Influence of the resin bath temperature on the measured data of the circumferential winding. The values are estimated for the complete video recorded (temperature profile at pixel 400, winding speed: 0.28 m/s)

by the interception of a line-region with the fiber-band edge. Then, from the first and second edge, an edge-line is mathematically defined for each pair of edge-points. In this way, the bandwidth corresponds to the magnitude of the perpendicular line from one of the edge-lines to the other (Figure 7). Furthermore, the winding-angle is formed by the bandwidth's perpendicular vector and a line-region. This method relies on the fiber-band edge recognition, and therefore, the accuracy of the measurements is dependent on its correct detection. Thus, a clear contrast between the fiber-band and the background is required.

Since the temperature decreases after the deposition, the contrast between the incoming fiber-band and the already deposited fiber (background) is achieved by a temperature difference.[20] Thus, a clear contrast has been characterized around ΔT equal to 8°C. Nevertheless, during the winding, a clear contrast cannot be always achieved, which difficult the accurate identification of the fiber-band. For these reasons, filter algorithms based on image gamma correction are implemented. Figure 8 shows an overview of the image processing algorithm. First, the IR-camera records a frame that is filtered by an initial gamma correction to reduce the illumination of the image (2. Gamma expansion). Then, a second gamma filter for the reconstruction of the image brightness is used (3. Gamma compression). Thus, an image with only the fiber-band can be obtained. Furthermore, an edge detection algorithm base on the watershed segmentation method is implemented.[51] Thus, the fiber bandwidth, and consequently the winding-angle, can be measured from the edge detection image (4. Edge detection).

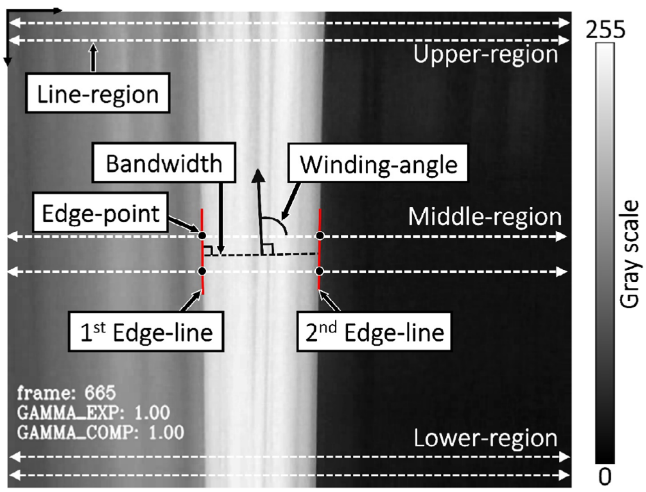

FIGURE 7 Estimation of the bandwidth and winding-angle at three different regions on the image: Upper, middle, and lower [Color figure can be viewed at wileyonlinelibrary.com]

4.1 | Gamma corrections

The gamma correction is defined by a non-linear optimization of the brightness expressed by Equation (1).[48–50] Then, an optimized image I_{out} is obtained from the input I_{in}, which is compensated by a gamma parameter γ and a constant parameter C.

$$I_{out} = CI_{in}^{\gamma} \tag{1}$$

In most cases, the brighter pixels belong to the incoming fiber-band, for example, higher temperature. Then, an initial gamma correction for the attenuation of the noise in the background is used. A gamma expansion

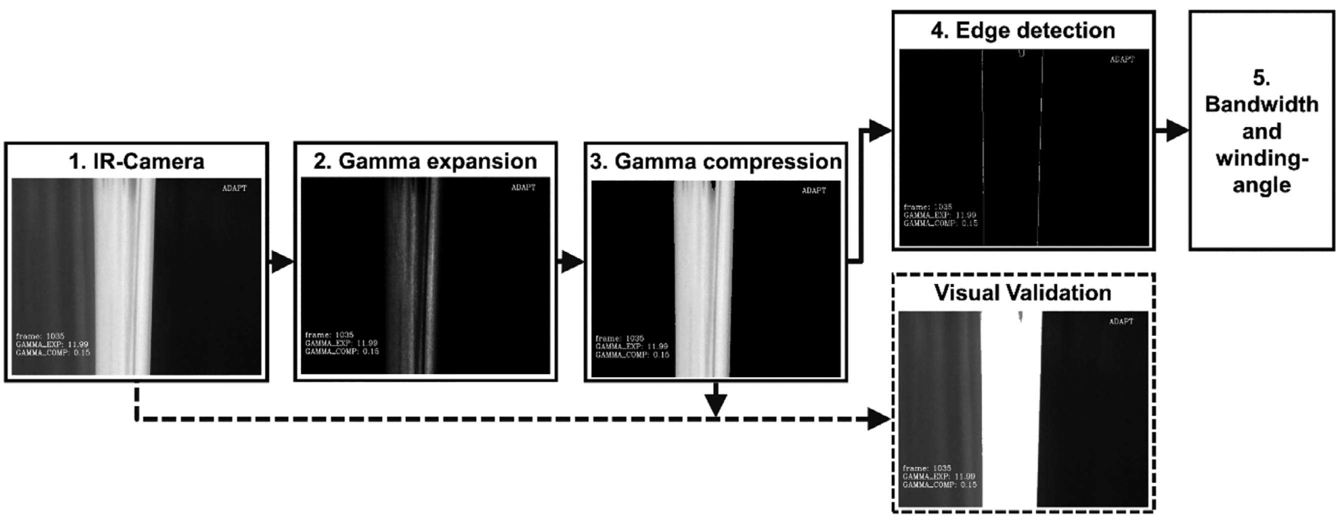

FIGURE 8 Image filter process based on gamma correction and edge detection for the estimation of the fiber bandwidth and winding-angle and visual validation of the gamma filter process (the enhanced image after the gamma compression is superposed on the image from the IF-camera)

parameter $\gamma_+ > 1$ is selected such that the illumination in the image is reduced (2. Gamma expansion). However, if a strong filter is applied, the information in the image can be lost and the correct estimation for the fiber bandwidth is hindered. Therefore, and opposite to the gamma expansion, a gamma compression parameter $\gamma_- < 1$ is selected for the enhancement of the image's brightness (3. Gamma compression). Then, the initial brightness of the incoming fiber is reconstructed without the background noise. In addition, for the validation of the fiber's edge detection after the gamma compression (4. Edge detection), the enhanced image from the gamma compression is superposed on the image obtained from IR-camera (Figure 8). Thus, any unsuitable variations in the detected fiber-band edge can be identified.

Furthermore, the correct combination of gamma parameters must be previously determined. This is usually made by empiric approaches where most of the recommendations have been proposed for images, rather than videos.[48,49] However, a video can be considered a sequence of images or so-called frames, where the gamma correction can be applied frame-wise. This represents a computational challenge for the image processing algorithm since the calculation must be made faster than the frame speed of the IR-camera. Thus, to guaranty a reasonable balance between computational time and information acquired, a compromise between the image-size and frame rate needs to be achieved. Thus, for an image of a size of 640×480 pixels, a frame rate of 30 fps is evaluated.

In this article, two implementations for the gamma correction are presented. First, a manual gamma correction, where constant values for γ_+ and γ_- are previously set up for all the frames. The parameter C correspond to a global scaling factor for all the pixel. Since the pixel value is restricted to grayscale (0, 255), any global scaling is normalized, and therefore, C does not influence this implementation. For simplicity, the parameter C is fixed to a value of 1. Then, the brightness variation for each frame is controlled only for the gamma parameter. However, a parameter study for the suitable selection of image processing parameters is required.

The second implementation for a gamma correction has been developed based on an adaptive algorithm.[49] Based on the distribution of pixels brightness, the algorithm calculates frame-wise a suitable combination of γ_+, γ_-, and C. Contrary to the manual implementation, the parameter C corresponds to a matrix where each pixel can be independently modified. In principle, an adaptive method implies a better correction frame-wise, compared to the manual correction. Nevertheless, the computational effort required must be evaluated.

4.2 | Parameter study for the manual gamma correction

A parameter study for the best combination of expansion and compression gamma parameters is performed. The gamma expansion parameter γ_+ regulates the attenuation of the noisy measurements in the background. Thus, γ_+ must be set up such as a good compromise between noise reduction and information loss is achieved. Three values for $\gamma_+ = (6.0; 12.0; 18.0)$ were evaluated. On the other hand, the gamma compression parameter controls the reconstruction of the initial brightness of the incoming fiber without the noisy measurements in the background. Thus, γ_- must be studied such as a suitable enhancement of the fiber-band is achieved. Three values for $\gamma_- = (0.05; 0.10; 0.50)$ are evaluated. Then, all the combinations among γ_+ and γ_- are evaluated (Figure 9).

A direct correlation between γ_+ and the attenuation of the brightness is observed. For $\gamma_+ = 6.0$ a poor noise reduction is achieved, which leads to an inaccurate estimation of the bandwidth and winding-angle. Hence, with the increment of γ_+, a clearer contrast of the fiber-band is obtained. On the other hand, an inverse correlation between γ_- and the brightness is observed. Thus, for lower values of γ_-, a brighter reconstruction of the fiber-band can be achieved. However, with very small values, any remained noise after the gamma expansion is highly amplified. From the validation images and using the configurations ($\gamma_+ = 12.0$, $\gamma_- = 0.1$) and ($\gamma_+ = 18.0$, $\gamma_- = 0.05$), a cleared fiber-band is observable (Figure 10). Nevertheless, a closer look at the configuration ($\gamma_+ = 18.0$, $\gamma_- = 0.05$) shows that the second edge in the fiber-band is repeatedly poorly reconstructed (red lines Figure 10).

Figure 11 shows the bandwidths and winding-angle estimations using the gamma configurations for the image validation. For the configuration with ($\gamma_+ = 12.0$, $\gamma_- = 0.1$), the upper region shows a larger bandwidth with an average value of 132 ± 15 pixels, while in the middle and lower regions, the average bandwidths are 125 ± 13 pixels, and 119 ± 12 pixels, respectively. For the other gamma configuration, the obtained average values are 115 ± 16 pixels, 113 ± 14 pixels, and 108 ± 13 pixels, for the upper, middle, and lower regions, respectively. Furthermore, an oscillation behavior of the values is observed. This behavior could be related to some process parameters. For instance, a drop in the fiber's tension. On the other hand, for the configuration with ($\gamma_+ = 12.0$, $\gamma_- = 0.1$), the results for the winding-angle show an average value of 89.2 ± 4.1, ° which agrees with the expected 90° winding-angle. Nevertheless, some dispersion is also observed, especially in the upper region. Contrary to the bandwidth, no oscillatory effect can be correlated with

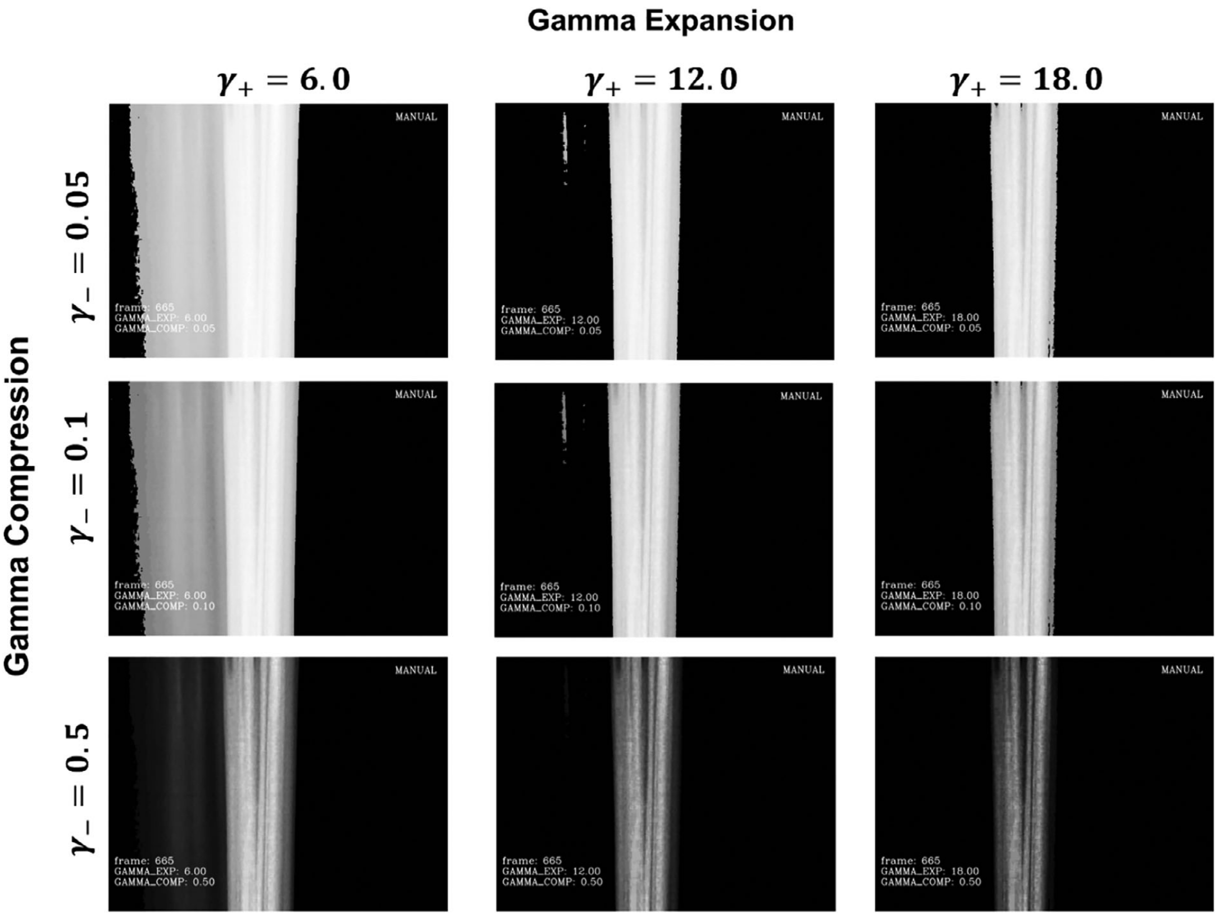

FIGURE 9 Parameter study for the manual gamma correction. $\gamma_+ = (6.0; 12.0; 18.0)$, $\gamma_- = (0.05; 0.10; 0.50)$. The images correspond to the gamma compression. (IR-images: 640 × 480 pixels)

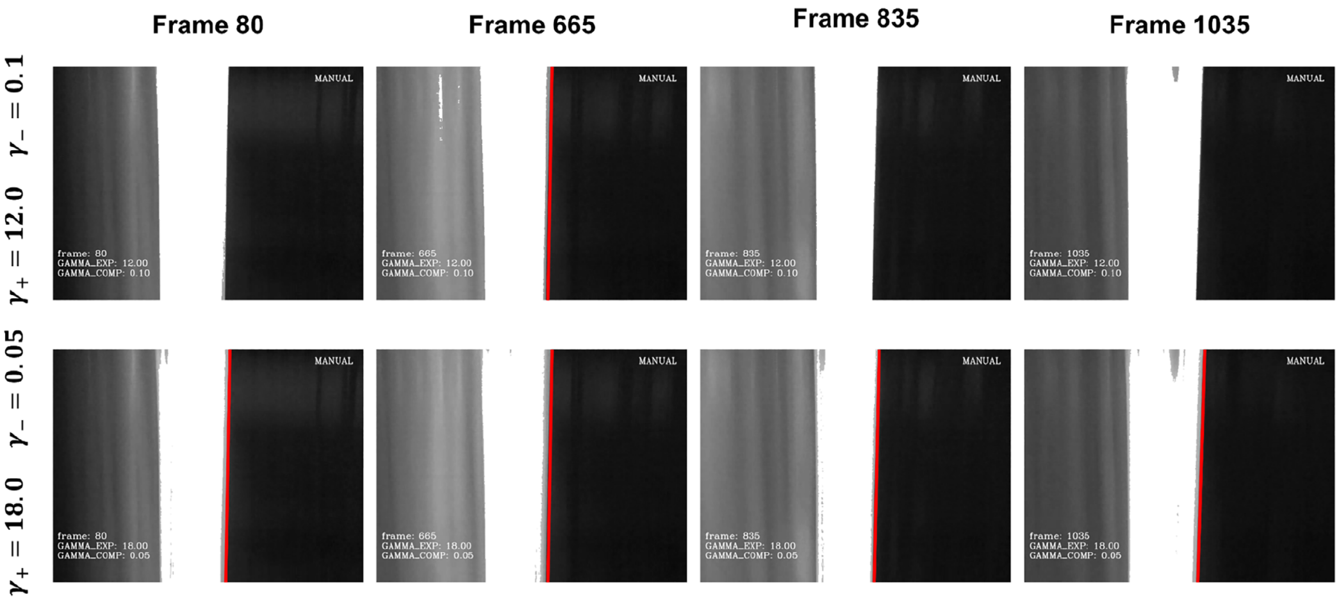

FIGURE 10 Validation of the manual gamma correction for the parameter configurations ($\gamma_+ = 12.0$, $\gamma_- = 0.1$) and ($\gamma_+ = 18.0$, $\gamma_- = 0.05$). The red lines show the real second edge in the fiber-band (IR-images: 640 × 480 pixels) [Color figure can be viewed at wileyonlinelibrary.com]

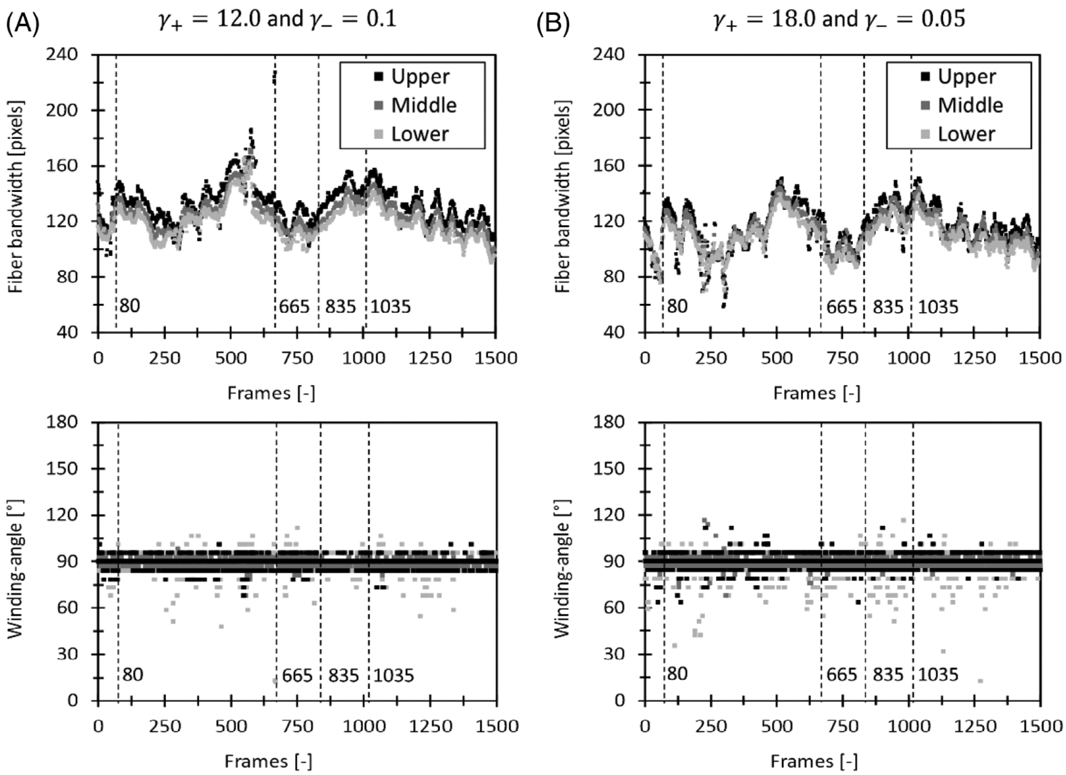

FIGURE 11 Bandwidth and winding-angle at three different regions on the fiber-band (see Figure 7). Two gamma parameters configurations (A) ($\gamma_+ = 12.0$, $\gamma_- = 0.1$) and (B) ($\gamma_+ = 18.0$, $\gamma_- = 0.05$)

the winding-angle. On the other hand, for the comparison of the two gamma configurations, punctual differences are obtained for some frames. Thus, a manual gamma correction does not always guaranty a correct measurement frame-wise.

4.3 | Adaptive gamma correction

Despite the good result from the parameter study, the manual implementation limits the image quality to a fixed condition. In reality, environmental and manufacturing conditions can variate, and therefore, a fixed parameter does not always guaranty a suitable image quality. Thus, an adaptive gamma correction based on the work from Rahman et al.[49] is implemented. In this way, the image in each frame is classified into lower or high contrast and a suitable gamma parameter is calculated. Nevertheless, the method has been only developed for a compression gamma enhancement. Thus, in this work, the inverse of the method is applied for the gamma expansion, Equation (2).

$$I_{out} = C I_{in}^{1/\gamma} \tag{2}$$

Consistent estimations of the bandwidth and winding-angle are obtained for the adaptive gamma method. For the three evaluated regions (upper, middle, and lower regions), the average values for the bandwidth 135 ± 16 pixels, 126 ± 14 pixels, and 121 ± 13 pixels are obtained (Figure 12(A)). Furthermore, the results for the winding-angle show an average value of $89.4 \pm 3.1°$, which also agrees with the expected winding-angle. The results obtained are comparable to the manual gamma correction with $\gamma_+ = 12.0$ and $\gamma_- = 0.1$. Figure 12(B) shows the variation frame-wise for the predicted expansion and compression gamma parameters. For the evaluated video, $\gamma_+ \approx 12$, while γ_- is quasi-constant with a value of around 0.15. Thus, the predicted gamma parameters are close to the suggestion for the parameter study. Thus, manual implementation is suitable to be applied. Nevertheless, the real conditions are prone to higher fluctuations of the process parameter, this can end up in not evaluated condition, where a fixed value for the gamma parameters is unsuitable. Thus, the exploration and optimization of the computational time in the adaptive gamma method is an option to be done. This adaptive method offers the advantage to obtain frame by frame the most suitable set of parameters for a well-defined contrast.

In comparison to the manual implementation, a drawback of the adaptive method is the frame-wise estimation of the gamma parameters which, increment the computational cost. Thus, the computational time of

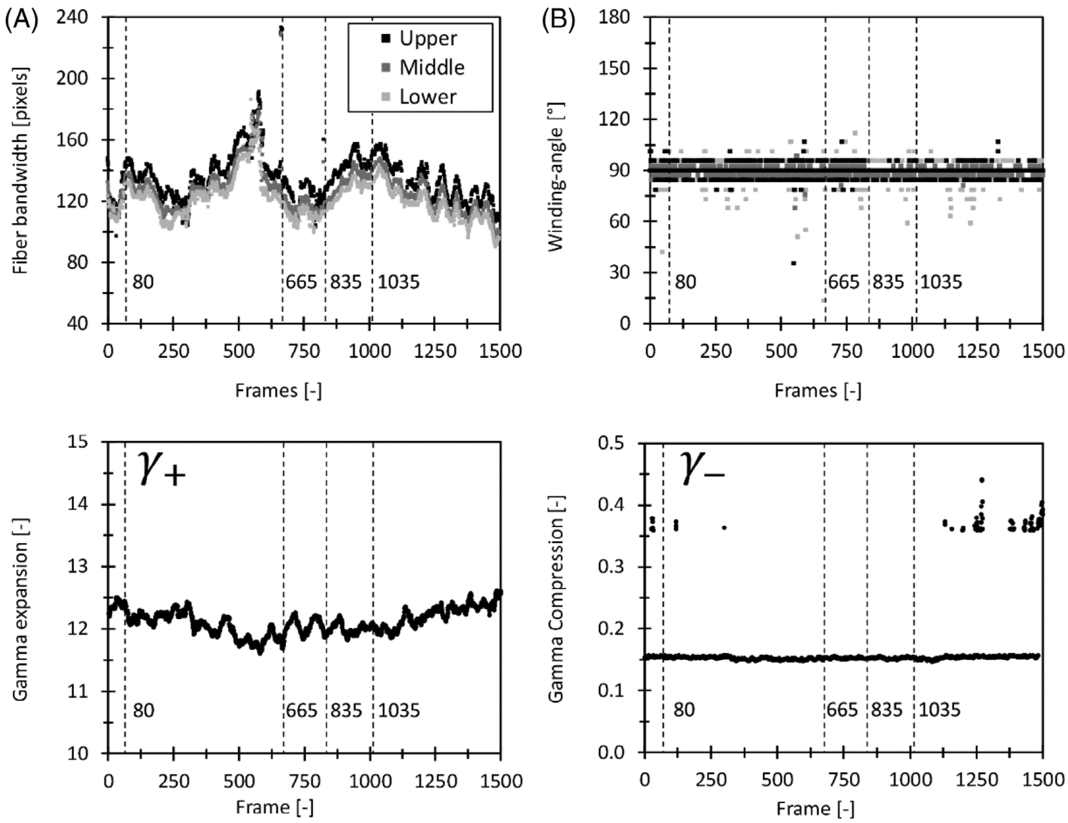

FIGURE 12 (A) Bandwidth and winding-angle measurements at three different regions on the fiber-band with adaptive gamma filter. (B) Gamma expansion and gamma compression parameters from the adaptive gamma filter

both gamma corrections methods is compared. To obtain a comparable measurement, both gamma corrections are tested in the same machine, without any optimization flag. Furthermore, the code run in a serial mode where only one processor core performed the whole calculation (AMD FX™-8350 Eight-Core Processor 4.00GHz). For the manual implementation, the average time required for the gamma correction, that is, gamma expansion plus compression, is 0.016 s. For the adaptive gamma correction, the average computational time is 0.078 s. Thus, the adaptive gamma correction required at least five times more computational time compared to the manual implementation. Furthermore, for a typical application, the IR-camera performs 30 frames/s or 0.033 s/frame. Thus, the manual implementation consumes almost half of the available computational time, while the adaptive implementation lay over the time boundary. It is important to remark that the adaptive gamma method has been developed for image enhancement and not for video applications. Then, a parallelization scheme for the optimization of the computational time is required. In addition, for the evaluated wet winding process conditions in this research, a frame rate of 30 fps can be considered a suitable recording speed.

5 | CONCLUSION

A new method based on an IR inline acquisition system to detect and evaluate the fiber-band during wet filament winding is investigated. The results show the suitability of the system for the determination of the fiber bandwidth and winding-angle during the deposition. However, the winding speed and resin bath temperature proved to influence the image quality. For the winding speeds between 0.28 and 0.96 m/s, no limitations regarding image processing were identified. Nevertheless, the derived trend indicates a lower image quality at winding speeds higher than 0.96 m/s, as well as for resin bath temperatures close to room temperature.

An image processing algorithm for the automatic detection of the fiber-band width and winding-angle during the winding process is developed. A manual gamma correction to improve the image contrast is evaluated. The parameter study showed that the wrong selection of gamma expansion and gamma compression parameters resulted in an inaccurate measurement of the bandwidth and winding-angle. Nevertheless, suitable parameters can be achieved. Since the manual gamma correction does not always guaranty a suitable image quality, an adaptive gamma method is implemented. The preliminary results showed that the adaptive method is able to find a correct set of gamma parameters frame-wise. However, the computational cost was five-time higher in comparison to the manual implementation. A frame rate of 30 fps can be considered a suitable recording speed.

Future work will focus on the integration of the inline measurement system into a robot-based winding equipment (Figure S2), allowing for higher winding speeds above 1 m/s and better process control. Moreover, this new winding technology enables the correlation of the machine position data with the inline measured fiber-band geometry for a 3D-visualization of the wound part.

ACKNOWLEDGMENTS

The research presented in this publication received financial support from the German Bundesministerium für Verkehr und Digitale Infrastruktur (BMVI) (No. 03B10104D). The authors extend their gratitude to BMVI, Projektträger Jülich (PtJ), and Now GmbH. Open Access funding enabled and organized by ProjektDEAL.

NOMENCLATURE

T	temperature
ΔT	temperature difference between the fiber-band and background
I_{out}	optimized image output
I_{in}	image input
C	scaling factor
γ	gamma parameter
γ_+	expansion gamma parameter
γ_-	compression gamma parameter

ORCID

Nicolas Rozo Lopez https://orcid.org/0000-0001-6085-628X

REFERENCES

[1] M. Munro, *Polym. Compos.* **1988**, *9*(5), 352.
[2] S. Peters, *Composite Filament Winding*, ASM International, Ohio **2011**.
[3] S. M. Lee, *Handbook of Composite Reinforcements*, VCH Publishers, New York, NY **1993**.
[4] M. Neitzel, P. Mitschang, U. Breuer, *Handbuch Verbundwerkstoffe*, Carl Hanser Verlag GmbH & Co. KG, München **2014**.
[5] A. Banerjee, L. Sun, S. C. Mantell, D. M. Cohen, *Compos. A: Appl. Sci. Manuf.* **1998**, *29*(3), 251.
[6] J. U. Almeida, H. L. Ornaghi, N. Lorandi, G. Marinucci, S. Amico, *Polym. Eng. Sci.* **2017**, *58*(10), 1837.
[7] C. Aleong, M. Munro, *Polym. Eng. Sci.* **1991**, *31*(18), 1344.
[8] G. DiVita, M. Marchetti, P. Moroni, P. Perugini, *Compos. Manuf.* **1992**, *3*(1), 53.
[9] E. Vargas-Rojas, D. Chapelle, D. Perreux, F. Thiebaud, *Compos. Struct.* **2014**, *116*(1), 805.
[10] Rice B. 700 Bar COPV Manufacturing - IACMI. Department of Energy Physical-Based Hydrogen Storage Workshop: Identifying Potential Pathways for Lower Cost 700 Bar Storage Vessels: IACMI; **2016**.
[11] N.N. Addendum 13: Global technical regulation No. 13 - Global technical regulation on hydrogen and fuel cell vehicles. United Nations; **2013**.
[12] C. Schmidt, B. Denkena, K. Völtzer, T. Hocke, *Procedia CIRP* **2017**, *62*, 27.
[13] Tait R, Harding K, Nafis C. Composite layup monitoring using structured light. Dimensional optical metrology and inspection for practical applications IV. **2015**;*9489*:1–9.
[14] D. P. Almond, W. Peng, *J. Microsc.* **2000**, *201*, 163.
[15] B. Denkena, C. Schmidt, K. Völtzer, T. Hocke, *Compos. Part B Eng.* **2016**, *97*, 239.
[16] J. A. Ritter, J. F. Sjogren, *Real-Time Infrared Thermography Inspection and Control for Automated Composite Material Layup United States*, The Boeing Company, Chicago, IL **2006**.
[17] Colas O, Courtemanche B, Reun AL. Online infrared thermography: Application to filament winding process defects detection. 14th Quantitative InfraRed Thermography Conf. Berlin, Germany, **2018**. 658–9.
[18] J. Park, C. Kim, J. Na, J. Yi, M. Turk, *Image Vision Comput.* **2008**, *26*, 1449.
[19] Sosnowski T, Bieszczad G, Madura H. Image processing in thermal cameras. Advanced technologies in practical applications for national security: Springer International; **2018**. p. 35–57.
[20] T. Bae, Y. Kim, S. Ahn, *Sensors* **2019**, *19*(11), 2455.
[21] J. Brüning, B. Denkena, M.-A. Dittrich, T. Hocke, *Procedia CIRP* **2017**, *66*, 74.
[22] T. K. Christ, *Rechnerische und experimentelle Untersuchungen zum Versagensverhalten CFK-umwickelter Kryo-Druckbehälter*, Technischen Universität München, München **2017**.
[23] Tonejc M, Steiner H, Fauster E, Konstantopoulos S, Schledjewski R. A study on geometrical parameters influencing the mechanical spreading of fibre bundles. 20th Int. Conf. on Composite Materials. Copenhagen, Denmark. **2015**.
[24] M. S. Irfan, V. R. Machavaram, R. S. Mahendran, N. Shotton-Gale, C. F. Wait, M. A. Paget, M. Hudson, G. F. Fernando, *J. Compos. Mater.* **2011**, *46*(3), 311.
[25] V. V. Vasiliev, *Composite Pressure Vessels: Analysis, Design, and Manufacturing*, Bull Ridge Corporation, Blacksburg, VA **2009**.
[26] A. Witte, *Einsatz optischer Messtechnik zur Qualitätssicherung eines Thermoplast-Wickelprozesses für die Faserverbundtankherstellung*, Apprimus, Aachen **2015**.
[27] R. Schmitt, A. Witte, *Proc. Manuf. Syst.* **2012**, *7*, 125.
[28] Colas O, Courtemanche B, Le Reun A. Online infrared thermography: Application to filament winding process defects detection. 14th Quantitative Infrared Thermography Conf. Quebec: Qirt Council; **2018**. 658–9.
[29] N. Miesen, J. Sinke, R. M. Groves, R. Benedictus, *Int. J. Adv. Manuf. Technol.* **2016**, *82*, 341.
[30] N. Miesen, R. M. Groves, J. Sinke, R. Benedictus, *Sensors Smart Struct. Technol. Civil Mech. Aerosp. Syst.* **2013**, *8692*, 1.
[31] R. Schmitt, C. Mersmann, B. Damm, *Opt. Photon. Digit. Technol. Multimed. Appl.* **2010**, *7723*, 1.
[32] C. Krombholz, D. Delisle, M. Perner, Advanced automated fibre placement. in *11th Int. Conf. on Manufacturing Research (ICMR2013)* (Ed: X. X. V. I. I. AiMT), Cranfield, Great Britain **2013**, p. 411.

[33] Krombholz C, Perner M, Bock M, Röstermundt D. Improving the production quality of the advanced automated fiber placement process by means of online path correction. 28th Int. Congress of the Aeronautical Sciences **2012**. 3922–31.
[34] Nguyen DC, Krombholz C, Röstermundt D. Einfluss einer online Bahnkorrektur auf die Materialeigenschaften von Prepreg Tows im Fiber Placement Prozess. DLRK2012. Berlin, Germany, **2012**.
[35] W. Faidi, *Wind Turbine Manufacturing Process Monitoring*, Niskayuna, NY, General Electric Global Research Center **2011**.
[36] B. Denkena, C. Schmidt, P. Weber, *Proc. Manuf.* **2016**, *6*, 96.
[37] C. Schmidt, C. Schultz, P. Weber, B. Denkena, *Compos. Part B Eng.* **2014**, *56*, 109.
[38] E. Gregory, P. Juarez, *J. Nondestruct. Eval. Diagn. Progn. Eng. Syst.* **2018**, *1*(4), 1.
[39] P. D. Juarez, K. E. Cramer, J. P. Seebo, *Therm. Infrared Appl.* **2016**, *9861*, 1.
[40] E. Oromiehie, B. G. Prusty, P. Compston, G. Rajan, *Struct. Health Monitor.* **2017**, *17*(1), 108.
[41] E. Oromiehie, B. G. Prusty, P. Compston, G. Rajan, *Compos. Struct.* **2019**, *224*, 110987.
[42] C. Krombholz, M. Bock, M. Perner, D. Röstermundt, M. Meyer, *Deutscher Luft-und Raumfahrtkongress* **2011**, 27.
[43] C. F. Vahlund, B. R. Gebart, *Polym. Compos.* **2001**, *22*(3), 327.
[44] H. Yang, J. S. Colton, *Polym. Compos.* **1994**, *15*(1), 46.
[45] F. Gadala-Maria, F. Parsi, *Polym. Compos.* **1993**, *14*(2), 126.
[46] I. J. Aldave, P. V. Bosom, L. V. González, I. L. de Santiago, B. Vollheim, L. Krausz, M. Georges, *Infrared Phys. Technol.* **2013**, *61*, 167.
[47] N. Rozo-Lopez, C. Hopmann, *SAMPE Europe* **2020**, *1*, 1.
[48] Z. Huang, T. Zhang, Q. Li, H. Fang, *Infrared Phys. Technol.* **2016**, *79*, 205.
[49] S. Rahman, M. M. Rahman, M. Abdullah-Al-Wadud, G. D. Al-Quaderi, M. Shoyaib, *EURASIP J. Image Video* **2016**, *35*(1), 2016.
[50] Li Y, Liu X, Liu Y. Adaptive local gamma correction based on mean value adjustment. 2015 Fifth Int. Conf. on Instrumentation and Measurement, Computer, Communication and Control. **2015**.
[51] K. V. Leemput, F. Maes, D. Vandermeulen, A. Colchester, P. Suetens, *IEEE Trans. Med. Imaging* **2001**, *20*(8), 677.
[52] C. Hopmann, F. Otremba, K. Fischer, N. Magura, J. Wipperfürth, F. Becker, F. Italiano, A. Girelli, D. Schneider, New methods for testing and quality assurance of high-performance FRP. 30th Int. Colloquium Plastics Technology. Aachen. **2020**.

SUPPORTING INFORMATION

Additional supporting information may be found online in the Supporting Information section at the end of this article.

How to cite this article: Hopmann C, Magura N, Rozo Lopez N, Schneider D, Fischer K. Detection and evaluation of the fibers' deposition parameters during wet filament winding. *Polym Eng Sci*. 2021; 1–15. https://doi.org/10.1002/pen.25649